Icarus 221 (2012) 300–309

Contents lists available at SciVerse ScienceDirect

Icarus

journal homepage: www.elsevier.com/locate/icarus

Determining meteoroid bulk densities using a plasma scattering model with high-power large-aperture radar data

Sigrid Close [a,*], Ryan Volz [a], Rohan Loveland [b], Alex Macdonell [b], Patrick Colestock [b], Ivan Linscott [c], Meers Oppenheim [d]

[a] Stanford University, Department of Aeronautics and Astronautics, 496 Lomita Mall, Stanford, CA 94305, United States
[b] Los Alamos National Laboratory, Space and Remote Sensing Sciences, Mail Stop D436, Los Alamos, NM 87545, United States
[c] Stanford University, Department of Electrical Engineering, 350 Serra Mall, Stanford, CA 94305, United States
[d] Boston University, Center for Space Physics, Boston, MA 02215, United States

ARTICLE INFO

Article history:
Received 16 November 2011
Revised 22 June 2012
Accepted 24 July 2012
Available online 13 August 2012

Keywords:
Meteors
Radio observations
Radar observations
Origin, Solar System

ABSTRACT

We present an improved technique for calculating bulk densities of low-mass (<1 g) meteoroids using a scattering model applied to the high-density plasma formed around the meteoroid as it enters Earth's atmosphere. These plasmas, referred to as head echoes, travel at or near the speed of the meteoroid, thereby allowing the determination of the ballistic coefficient (mass divided by physical cross-section), which depends upon speed and deceleration. Concurrently, we apply a scattering model to the returned signal strength of the head echo in order to correlate radar-cross-section (RCS) to plasma density and meteoroid mass. In this way, we can uniquely solve for the meteoroid mass, radius and bulk density independently. We have applied this new technique to head echo data collected in 2007 and 2008 simultaneously at VHF (160 MHz) and UHF (422 MHz) at ALTAIR, which is a high-power large-aperture radar located on the Kwajalein Atoll. These data include approximately 20,000 detections with dual-frequency, dual-polarization, and monopulse (i.e. angle) returns. From 2000 detections with the smallest monopulse errors, we find a mean meteoroid bulk density of 0.9 g/cm^3 with observations spanning almost three orders of magnitude from 0.01 g/cm^3 to 8 g/cm^3. Our results show a clear dependence between meteoroid bulk density and altitude of head echo formation, as well as dependence between meteoroid bulk density and 3D speed. The highest bulk densities are detected at the lowest altitudes and lowest speeds. Additionally, we stipulate that the approximations used to derive the ballistic parameter, in addition to neglecting fragmentation, suggest that the traditional ballistic parameter must be used with caution when determining meteoroid parameters.

1. Introduction

A meteoroid is defined as a solid object moving in interplanetary space, of a size considerably smaller than an asteroid and considerably larger than an atom. Smaller particles are termed "dust" and larger particles are termed "asteroids". Though this definition is often used loosely, it has defined a research area that has been active since people began counting shooting stars, or meteors, that form in our atmosphere. These meteors, which are the plasmas formed in our atmosphere when meteoroids collide with the background atmosphere, are the primary measurement for meteoroid research. A small subset of meteoroid research results from direct measurements of the meteoroid through impacts with spacecraft (Love and Brownlee, 1993). The primary observing tool for meteors includes ground-based optical and radar systems.

While low-power radar have been used to collect meteor data since the late 1940s, during the past 20 years the use of high-power, large-aperture (HPLA) radar have become an equally important instrument for meteor observations. HPLA radar data have provided new insights into the field of meteor physics (Chapin and Kudeki, 1994; Wannberg et al., 1996; Zhou et al., 1998; Janches et al., 2000; Close et al., 2004; Oppenheim et al., 2008; Mathews et al., 1997; Sugar et al., 2010). In particular, HPLA radars routinely detect the head echo, which is the plasma that surrounds a meteoroid and is believed to travel at its velocity. In this way, one of the key observables of the meteoroid (i.e. the velocity) is immediately determined and can be used in conjunction with other observables to determine meteoroid properties. This somewhat simplifies the very difficult problem of correlating the observed plasma properties to the desired, but inferred, meteoroid properties.

When studying meteoroids, it is often desirous to obtain (in addition to the velocity) the mass of the meteoroid. This often proves to be a difficult problem, however. If we conserve momentum between

* Corresponding author.
E-mail address: sigridc@stanford.edu (S. Close).

0019-1035/$ - see front matter © 2012 Elsevier Inc. All rights reserved.
http://dx.doi.org/10.1016/j.icarus.2012.07.033

the meteoroid and the air molecule, we can derive a quantity called the ballistic parameter, which is the meteoroid mass divided by the cross-sectional area. By assuming a meteoroid bulk density, we can then infer a meteoroid mass (Close et al., 2000; Janches et al., 2000). However, besides the obvious need to guess a density, this approach also assumes "single-body theory" whereby the meteoroid impacts air molecules through a series of independent collisions. It also does not include effects such as fragmentation and differential ablation (Janches et al., 2009), both of which are further obscured by poorly-understood plasma processes such as polarization-dependent scattering mechanisms (Close et al., 2011; Wannberg et al., 2011). An alternative method is to use the signal strength, or radar-cross-section (RCS) of the scattered plasma to determine meteor plasma density (Close et al., 2004; Dyrud and Janches, 2008; Szasz et al., 2008). Plasma density can then be directly correlated to meteoroid mass loss rate by assuming an ionization probability, which is determined primarily from laboratory measurements. This method relies on a scattering model that incorporates head echo size and shape, but does not require the assumption of a meteoroid mass or radius.

In this paper, we present a technique that incorporates both the conservation of momentum together with electromagnetic scattering from plasmas in order to uniquely determine not only the meteoroid mass, but the meteoroid bulk density and radius as well. Our method refines the technique of Drew et al. (2004) by employing a new ballistic mass model and incorporating higher quality radar measurements and signal processing (Loveland et al., 2011) to provide the most accurate meteoroid bulk densities yet observed for the small, fast meteoroids detected by HPLA radar.

Section 2 gives a brief review of the high-resolution, multi-frequency ALTAIR head echo data set. In Section 3, we provide an overview of our models, including the spherical scattering model and a modified ballistic parameter model. Section 4 contains an overview of our analysis and a discussion of our results. Section 5 summarizes and expands upon future work.

2. ALTAIR head echo data

ALTAIR is an HPLA radar that resides in the central Pacific at 9°N and 167°E (geographic) on the island of Roi-Namur in the Kwajalein Atoll, Republic of the Marshall Islands. This site is named the "Reagan Test Site" and is host to various instruments used for monitoring space surveillance activities as well as ballistic re-entry tests. The Reagan Test Site is also used for dedicated scientific experiments funded by agencies such as NASA. The data described herein were collected under this last umbrella.

ALTAIR transmits a peak power of 6 MW simultaneously at the two frequencies with right-circularly (RC) polarized signal energy in a half-power beamwidth of 2.8° and 1.1° at VHF and UHF, respectively. The typical operating frequencies include 160 MHz and 422 MHz. ALTAIR receives both right-circular (RC) and left-circular (LC) energy and has four additional receiving horns for the purpose of angle measurement. This monopulse feed system uses a form of amplitude-comparison in order to correct for the object's location within a range gate and provide the object's position, speed, and deceleration in three dimensions.

Radar meteor data were collected simultaneously at VHF and UHF at ALTAIR in 2007 and 2008 and include approximately 30 h of data. Both head echoes and trails were observed throughout the year-long collection period, which included sporadic data collects typically centered around 6 AM local time in order to span the time-frame of Earth's orbit. Amplitude and phase data were recorded for each frequency and four receiving channels for altitudes spanning 80–140 km. The two ALTAIR waveforms used to collect the data were a 100 μs VHF chirped pulse ("V7100") with 15-m range spacing, and a 150 μs UHF chirped pulse ("U7100") with 15-m range spacing. These waveforms were chosen because of their high-sensitivity and high range resolution. A 115 Hz pulse-repetition frequency (PRF) was utilized due to ALTAIR system requirements associated with these two waveforms. Using these waveforms, ALTAIR can detect a target as small as −50 decibels-relative-to-a-square-meter (dBsm) at VHF and −65 dBsm at UHF at a range of 100 km (Janches et al., 2008).

We used a head echo detection method based on the Delaunay triangulation in order to automatically search through the 30 h of data, a period of time corresponding to roughly 10^5 head echoes. The head echo range rates and 3D speeds were derived by applying a new phase-derived matching technique, described in Loveland et al. (2011). This new technique reduced the error in the range rate to on the order of 1 m/s.

3. Methodology

We implement two models in order to uniquely solve for meteoroid mass, bulk density, and radius as a function of altitude. The first includes a plasma scattering model of the head echo, first described in Close et al. (2004). The second is a modified version of the familiar ballistic parameter that now includes terms related to the ablated atom. These models are described in this section.

3.1. Scattering mass

In order to derive a scattering mass, we model the interaction of the electromagnetic wave with the head echo plasma and calculate the plasma density and then use an ionization model to correlate the plasma density to a mass loss. This approach is described herein.

3.1.1. Spherical scattering model

We have slightly modified the scattering model described in Close et al. (2004) and Close et al. (2005) for application to the 2007 and 2008 ALTAIR data. This model calculates the scattering from head plasma and assumes the following: (1) the reflecting component of head plasma can be approximated as spherically symmetric; (2) the head plasma's radius depends upon altitude and scales with the atmospheric mean free path and meteoroid speed; (3) the head plasma density behaves as a Gaussian function; (4) we ignore both the $\vec{v} \times \vec{B}$ component of the Lorentz force due to the motion in the geomagnetic field, as well as any collisional terms in the ionosphere, since both the gyrofrequency and the collisional frequency in the E-region are negligible compared to the VHF and UHF frequencies, and the field is not high enough to drive electrons to relativistic speeds. Our goal is therefore to take the measured ALTAIR head echo RCS data and determine peak head plasma density.

Head echo RCS depends upon the peak plasma density, plasma density profile, and the size of the head plasma. Our approximation of the head plasma density, $n(r)$, is a Gaussian function of radius,

$$n(r) = n_{\max} \exp(-(r/r_{\max})^2) + n_b \quad (1)$$

where $n_{\max}$ is the maximum plasma density for each head plasma (near the meteoroid's position at the center of the head plasma), r is the radial distance from the center of the head plasma, $r_{\max}$ defines what we call the "physical size" of the head plasma and n_b is the background plasma density at the altitude of formation. We expect the size of the head plasma to scale approximately with the atmospheric mean free path for two reasons. First, the meteoroid ablates and sheds particles, some of which ionizes after colliding with neutral molecules, freeing the electrons principally responsible for the radar echo (Popova, 2004). Hence, as the mean free path

decreases, so will the size of the ionized region. Second, the gas and plasma released from a meteoroid expands largely without inhibition until it reaches, on average, a distance roughly equaling the mean free path; at this point, it will expand at a slower diffusive rate. The transition distance is called the initial radius and has been used extensively by researchers examining specular trails. As in Close et al. (2004), we choose our head radius, r_{max}, to be .023 times the Jones formula (Jones, 1995) or

$$r_{max} = (.023) * (2.845) \times 10^{18} v^{0.8}/n) \quad (2)$$

where v is the 3D speed of the head echo in km/s and n is the background number density at the head echo detection altitude in m^{-3}. The scaling factor of .023 was determined empirically from our dual-frequency observations: we iterate on the radius until the two plasma densities output from the scattering model match at both frequencies. We refer to Eq. (2) as the modified Jones formula. In order to determine the correlation between the reflection coefficient, R_n, and the plasma density, we derived a formula based on electromagnetic scattering from a sphere. This model used an electrostatic approximation to the full-wave solution for scattering from a diffuse plasma and is described in Close et al. (2004). For a head plasma with a size defined by Eq. (2), the reflection coefficient is given by

$$-\frac{1}{R_n} \cong 2 - \frac{nh_n^2(kr)A_n r^{2n+1}}{(n+1)j_n(kr)B_n} \quad (3)$$

where A_n and B_n are the coefficients determined by boundary conditions, j_n is the nth order Bessel function of the first kind, and h_n^2 is the nth order Hankel function of the second kind. Eq. (3) provides a link between the head echo peak plasma density and the reflection coefficient that is received by the radar. After performing numerical integration to calculate R_n, we relate R_n to a possible RCS, σ, such that

$$\sigma = \sum_n \frac{\lambda^2 \left(n+\frac{1}{2}\right)^2}{\pi} \cdot |R_n|^2 \quad (4)$$

where λ is the radar wavelength (Jackson, 1975; Morse and Feshbach, 1953). Since we do not know the peak plasma density, we choose values from a range of possible plasma densities and calculate σ for each of these possibilities. We then compare our measured RCS, after correcting for position within the beam, for each head echo as a function of altitude against the full range of possible RCS. The best fit provides the plasma density of that head echo. The beam pattern of the radar dominates the RCS dependence on time and altitude; it is therefore crucial that the beam pattern be removed from the head echo RCS. This model was validated using head echoes detected simultaneously at two frequencies since RCS is dependent upon radar frequency but plasma density is not. Because each separate radar frequency produces the same or a similar plasma density, we conclude that the model is self-consistent and the plasma densities are trustworthy.

3.1.2. Line density and mass loss

In order to determine the meteoroid mass from the scattering equations, we convert the peak plasma density of each head echo that is output from the scattering model, n_{max}, to a plasma line density, q. For meteor trails, q is constant at a constant altitude. For head echoes, however, q depends strongly on r and varies as a function of r up to its maximum radius, r_{max}. We therefore use an average line density (q) for subsequent use in our calculations, which is approximated by the discrete sum

$$q = \frac{1}{N} \sum_{r=0}^{r=r_{max}} n(r)\pi r^2 \quad (5)$$

where $n(r)$ is the plasma density at radius r, r_{max} is given by Eq. (2), and N is the number of steps between $r = 0$ and $r = r_{max}$.

The ALTAIR line densities, calculated using the spherical weighting, are then input into the standard meteoroid mass loss equation to determine meteoroid mass

$$\frac{dm_m}{dt} = \frac{q\mu v}{\beta} \quad (6)$$

where dm_m/dt is the meteoroid mass loss, μ is the mean molecular mass, which is approximately 20 for cometary meteoroids dominated by 60% oxygen and 25% silicon (Jones, 1997), v is the head echo speed and β is the ionization probability which depends upon the velocity and is given by Jones (1997). By summing the mass loss along the entire head echo streak, we can estimate the total mass as well as the mass loss as a function of altitude.

3.2. Ballistic mass

We begin with a derivation of the ballistic parameter using the conservation of momentum between the air molecule and the impinging meteoroid. While the ballistic parameter (meteoroid mass divided by cross-section) has been routinely used in the literature in order to determine meteoroid mass loss by assuming a meteoroid density, it often creates confusing results when evaluated over the length of the head echo/meteoroid streak (Bass et al., 2008; Close et al., 2005; Janches et al., 2000). We believe that the ballistic parameter must be used with caution for ablating meteoroids where the mass loss can be both differential and extreme, especially at the end of the meteoroid's life (Vondrak et al., 2008; Janches et al., 2009). To this end, we derive the ballistic parameter equation in order to explicitly show the assumptions and where we can relax these assumptions in this and future work.

The meteoroid and air molecule collide and conserve linear momentum, such that

$$m_a v_a + m_m v_m = (m_m - dm_m)(v_m - dv_m) + m'_a v'_a + dm_m v_{ab} \quad (7)$$

where the terms describing the system before the collision include m_m, the meteoroid mass, m_a, the air mass, v_m, the meteoroid velocity and v_a, the air velocity. Immediately after collision the meteoroid loses some mass, dm_m, as well as some velocity, dv_m, and the ablated particle, dm_m, travels at an unknown velocity, v_{ab}. Additionally, the air molecule's velocity and mass after collision is denoted by v'_a and m'_a. This equation is often analyzed in the reference frame of the air ($v_a = 0$) and simplified according the following assumptions: (1) $m'_a = m_a$, (2) $v'_a = \gamma v_m$ where γ is the drag coefficient, (3) $v_{ab} = v_m$, and (4) $dm_m * dv_m$ is small and can be ignored. Furthermore, if the amount of air mass that the meteoroid encounters per time (dt) is written as

$$\frac{m_a}{dt} = \sigma \rho v_m \quad (8)$$

where σ is now the physical cross section of the meteoroid ($\sigma = \pi r_m^2$) and ρ is the air density, then the ballistic parameter (mass over cross section), often quoted in literature, is simply

$$\frac{m_m}{\sigma} = \frac{\gamma \rho v_m^2}{\frac{dv_m}{dt}}. \quad (9)$$

Two primary issues with this equation arise when dealing with meteoroid mass loss. First, we do not know the speed of the ablated particle, v_{ab}, and second, the term often neglected ($dm_m * dv_m$) can become comparable to the size of the meteoroid at the end of its life or when undergoing differential ablation. If we replace assumption (3) with $v_{ab} = \eta v_m$, and remove assumption (4), we are left with

$$m_m - dm_m - \frac{dm_m}{dv_m} v_m(\eta - 1) = \frac{\gamma \sigma \rho v_m^2}{\frac{dv_m}{dt}}. \quad (10)$$

This equation shows that even for η close to 1, the additional two terms may make the more simplistic ballistic parameter invalid over the entire life of the head echo streak, as will be shown in the following sub-sections.

3.3. Meteoroid bulk density

We have two equations that can be used to solve for mass: the scattering mass (Eq. (6)), and by assuming a physical cross-section or a meteoroid bulk density, the ballistic mass (Eq. (10)). From the density relation for an object, we have a third equation for a spherical mass, namely

$$m_m = \frac{4}{3}\pi r_m^3 \delta \tag{11}$$

where δ is the meteoroid bulk density and r_m is the meteoroid radius. We can also modify this to include a shape factor to account for non-spherical meteoroids; this factor has been shown to be irrelevant for all but the largest meteoroids. We now have three equations (Eqs. (6), (10), and (11)) and three unknowns, including the meteoroid mass (m_m), radius (r_m) and bulk density (δ), allowing us to uniquely solve for all meteoroid parameters for the first time.

4. Analysis and discussion

In this section we provide the results of the ALTAIR data analysis by highlighting our methodology, as applied to a single head echo streak, followed by the statistics over approximately 20,000 meteoroids. The data contained herein include only VHF detections, which provide higher overall RCS values as well as a longer duration due to the wider beam. A discussion on the dual-frequency events is provided in a forthcoming paper.

4.1. Single head echo streak

The ALTAIR radar has a 4-horn monopulse feed system, which is the critical element for determining scattering and ballistic mass. Specifically, we not only use the monopulse data to correct for the head echo's position within the range gate, thereby providing a 3D position, velocity, and deceleration of the meteoroid, but we also use the monopulse to correct for the beam pattern that is evident in the RCS data. We provide an example of our methodology for determining meteoroid mass, radius and density by using a single head echo streak/meteoroid.

Fig. 1a shows the path of the head echo in azimuth and elevation, color-coded for LC RCS. The angles are relative to radar beam center, with 0° corresponding to the center of the ALTAIR beam. The RCS appears to be strongest closest to 0° elevation, suggesting that the primary contribution to the RCS dependence on altitude arises not from the plasma, but from the plasma's position within the beam. Fig. 1b shows a clearer example of the RCS, including both the LC and RC returns, as a function of altitude. The radar beam pattern is evident, with a slight dip near 105 km in both polarizations. Since RCS is calculated from the target signal-to-noise ratio using a conversion factor based on the antenna gain at the center of the beam, the measured RCS varies according to the beam pattern and is incorrectly lower for signals not in the center of the beam. However, because we know the radar beam pattern through calibration testing and the meteor position within the beam through monopulse measurements, we can correct the RCS data so that each measurement represents the true RCS. It is from the corrected RCS data that we calculate the scattering mass. We note that although this correction could introduce additional RCS error due to errors in monopulse measurements, we nevertheless expect a net gain in RCS accuracy over the uncorrected measurements. Fig. 1c shows the speed of the head echo/meteoroid, including both the range rate (RR) as well as the monopulse-corrected range rate using the interpulse Doppler method of Loveland et al. (2011), which we call 3D. Note that since this particle was traveling primarily "down-the-beam", or parallel to the ALTAIR radar boresite, the difference between 3D speed and range rate is minimal. Next we apply the scattering model to calculate meteoroid mass (Eq. (6)) as a function of altitude, which is shown in Fig. 1d. This mass, including the mass loss term, is input into Eq. (10) to calculate the meteoroid radius, which is shown in Fig. 1e, and then both the mass and the radius are used to calculate the meteoroid density, using Eq. (11). The meteoroid density as a function of altitude is shown in Fig. 1f. Both the radius and the density appear to have a slight non-physical curvature, but this level of error is reasonable given the approximations of the model and the accuracy of the radar measurements. Many head echoes display a constant density with altitude, which given the physics of meteoroid ablation is to be expected, while some show a dramatic (factor of 2–3) change in meteoroid density as a function of altitude. Nevertheless, we believe that these represent the highest accuracy HPLA radar measurements yet made of a meteoroid's mass, radius and density.

4.2. Detection statistics

We applied the method just described to a subset of the 2007/2008 data set, which includes approximately 20,000 head echoes detected at VHF. As noted earlier, these data were collected primarily centered on 6 AM local time in order to maximize the number of detections (Janches et al., 2006). The pointing of the ALTAIR beam, color-coded for local time, is contained in Fig. 2.

Although our search and analysis technique is automated, we analyzed a subset of the data by hand in order to ensure that our modeling and calibration of the RCS was representative of the types of signals. In particular, we examined the dual-polarized RCS signals to look for trends. Unexpectedly, we could apply no generalizations to the RCS dependence with altitude over the thousands of head echoes that we analyzed. While the LC RCS was greater than the RC RCS for the majority of the individually-analyzed head echoes, there were many instances where the RC RCS was comparable to the LC. Additionally, very few head echoes were "smooth"; most contained sharp increases and decreases that were often, but not always, seen in both polarizations. Some representative RCS curves are shown in Fig. 3. Fig. 3a shows what we call a smooth RCS profile with the LC clearly stronger than the RC; Fig. 3b shows a similar trend but with a sharp jump in both polarizations, most likely due to differential ablation (Janches et al., 2009). Fig. 3c and d show interesting polarization features, with structure only seen in the RC (Fig. 3c) or the LC (Fig. 3d). Fig. 3e and f show returns where the strength is comparable in both polarizations with a periodic behavior seen throughout the signal.

We begin a generalized introduction to the properties of these approximately 20,000 head echoes by showing the histogram of the LC and RC RCS returns; this is shown in Fig. 4a. As discussed in Close et al. (2002), more than 50% of the head echoes detected in 1998 and 1999 show a high polarization ratio with the LC much stronger than RC – consistent with scattering from an object that is either sphere-like or plate-like (i.e. equal lengths in both the x and y directions relative to a wavelength propagating in the z direction). We perform the same analysis for this data set. Since the polarization ratio can change along the length of the head echo streak, we divide the maximum LC signal by the maximum RC signal of the streak, noting that these maxima could occur at different altitudes; this approach is preferred since noise at any one time can cause spuriously high or low polarization ratios. The normalized polarization ratio, calculated by taking the maximum polarization difference possible and dividing by the

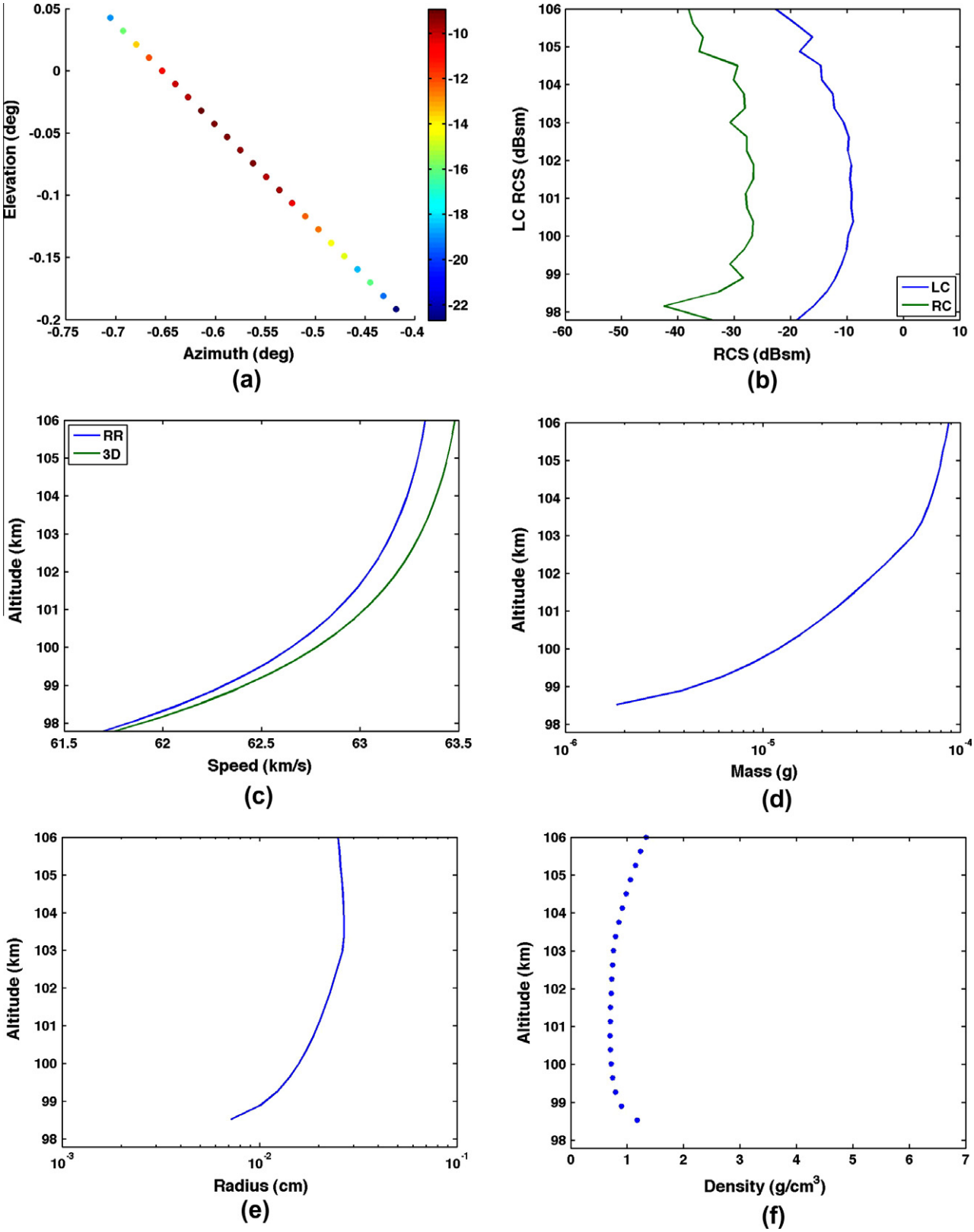

Fig. 1. A single head echo streak/meteoroid showing the methodology for determining meteoroid mass, radius and density from head echo plasma. (a) Monopulse azimuth and elevation offset from radar beam center (resulting from a fit assuming the meteor travels along a straight path), color-coded for LC RCS, (b) the dual-polarized RCS returns in LC and RC as a function of altitude, (c) the speed as a function of altitude for both the range rate (RR) and the monopulse-corrected range rate, which is the 3D speed (3D), (d) the meteoroid mass as a function of altitude, (e) the radius of the meteoroid as a function of altitude, and (f) the meteoroid density as a function of altitude.

polarization difference observed, is shown in Fig. 4b. The mean normalized polarization ratio for these approximately 20,000 head echoes is 1.57. The maximum polarization ratio is governed by 2 factors. These include (1) the slight ellipticity of the ALTAIR feed

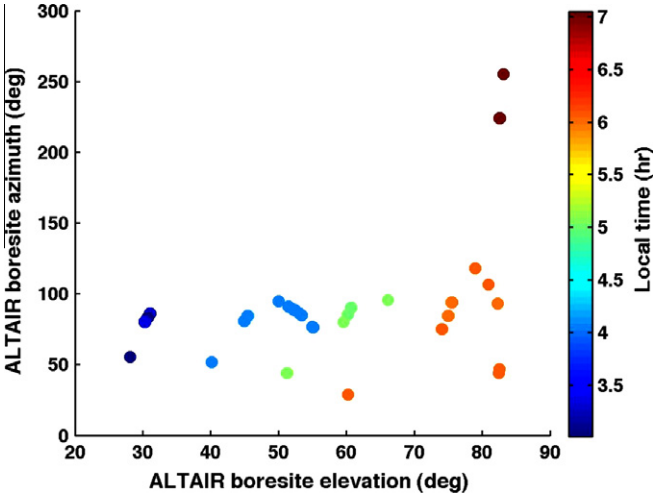

Fig. 2. ALTAIR boresite azimuth and elevation pointing for the 2007/2008 data collect, color-coded for local time.

horn, which makes the maximum polarization 20 dBsm, which limits the overall maximum polarization ratio, and (2) the sensitivity of the system, which limits the maximum polarization for head echoes that have SNR near the noise floor. As an example of this normalization calculation, consider a head echo with a peak LC RCS of −45 dBsm and a peak RC RCS of −50 dBsm, which gives a polarization difference of 5 dBsm. Given that ALTAIR's limiting sensitivity is −50 dBsm (for the waveform used in these experiments), the maximum polarization difference (assuming the RC is always smaller) is 5 dBsm; therefore the normalized polarization ratio is 1. As another example, we consider a head echo with a peak LC RCS of −20 dBsm and a peak RC RCS of −25 dBsm, which gives a polarization difference of again 5 dBsm. However since we are not near the noise, the maximum polarization is now governed by the capability of the system and is 20 dBsm. Therefore the normalized polarization ratio is four. Therefore, normalized polarization ratios above 1 correspond to "non-ideal" scattering, meaning those that are returning higher RC than expected for a perfect reflector. Negative normalized polarization ratios, which include 89 head echo streaks or less than 1% of detections, correspond to those with RC higher than LC. Many factors can contribute to non-idealities, including noise in the signal, a varying polarization difference with altitude, fragmentation, etc. These effects are discussed in Vertatschitsch et al. (2011) and Close et al. (2011).

Fig. 4c contains the histogram of the maximum altitude of each head echo detected at VHF, which spans the full range window of 80 km through 140 km. Unlike the 1998/1999 data, there appears to be a sharp edge to the histogram near 110 km, which is consistent with a frequency-dependent scattering mechanism (Close et al., 2005; Mathews, 2004; Westman et al., 1997; Westman et al., 2004). As the altitude increases, the mean free path, and hence the "size" of the head plasma increases. At some point, very similar to the initial trail radius, the size of the head plasma will exceed the wavelength. At 110 km, the mean free path is approximately 1 m, or approximately half the radar wavelength. Above these altitudes, the plasma will begin to look underdense at this particular frequency, thereby decreasing the likelihood of detection. Fig. 4d shows the histogram of head echo velocity angles with respect to the ALTAIR boresite; the mean angle is 33°, which indicates that observations using radars that lack an interferometric or monopulse system (e.g. Arecibo) contain only a small error by assuming that meteoroids travel parallel to the radar beam.

4.3. Meteoroid masses and bulk densities

We characterize the meteoroid masses and bulk densities as a function of velocity and altitude for 2000 meteoroids with the smallest errors in azimuth and elevation offset (<0.1σ). As described in Close et al. (2007), selection effects that are inherent to every observing system will bias the detected population to those with more energy. HPLA radars also suffer from this effect, although to a lesser degree than low-power, specular radars. Regardless, each instrument has a limiting sensitivity, which by definition defines an absolute energy cutoff of the meteoroid; a meteoroid with energy below that threshold will be undetectable by the system (Janches et al., 2008).

Fig. 5a shows the maximum LC RCS in dBsm of each head echo as a function of the maximum altitude of detection, color-coded for the $\log_{10}$ of the meteoroid mass that was calculated using the scattering model. The size of the circle corresponds to the maximum 3D speed of each meteoroid, such that large circles correspond to fast meteoroids, while small circles correspond to slow meteoroids. The meteoroids with the largest masses and highest speeds form head echoes with large RCS values at high altitudes. Meteoroids with low masses and large speeds are still formed at the highest altitudes, but with lower RCS values. The smallest RCS values correspond to low mass, low speed particles. This figure is in agreement with previous results (Mathews et al., 2008; Janches et al., 2003; Stober et al., 2011) and most notably, shows the ionization probability scaling with velocity: the highest speed meteoroids will create head echoes at the highest altitudes.

Fig. 5b shows the same data, now plotted as the $\log_{10}$ of the plasma line density as a function of altitude, color-coded for the $\log_{10}$ of the scattering mass; the size of the circle corresponds to the maximum 3D speed of each meteoroid. This plot reveals an expected result – namely a velocity selection effect. Once again the highest-mass meteoroids create the largest plasma line densities, but only for relatively high speeds. At low altitudes (<100 km), we can only detect low-speed particles if the masses are high. This is shown by the far left side of the curve at altitudes below 100 km. At these altitudes, as the meteoroid speed increases, we can detect smaller and smaller particles (cyan-green colored meteoroids). This abrupt distinction near 100 km is only evident when plotting the head echo altitude as a function of line density and not RCS, which supports the theory that the RCS results from both the line density and the size of the head echo. In particular, for a given meteor the line density will increase dramatically as it descends before decreasing over a small altitude extent, whereas the size of the head echo will continually decrease as it descends – consistent with the change in the atmospheric mean free path.

Fig. 6a contains a histogram of the meteoroid bulk densities; the mean is 0.9 g/cm^3. Any non-physical densities, which comprise 5–10% of the data, were removed. The highest density meteoroids have densities consistent with the measured meteorites of McCausland et al. (2011) and relative populations consistent with the optical meteor measurements of Kikwaya et al. (2011). Once again selection effects are evident, since compared to these other methods, our HPLA radar approach allows measurement of meteoroids with lower densities that either do not reach the Earth's surface or do not result in significant optical emission. Fig. 6b shows the meteoroid densities as a function of 3D speed and altitude. This plot is most striking and clearly shows that higher speed meteoroids form plasma at higher altitudes and that the spread in particles in altitude at any one speed corresponds to the differences in meteoroid density. For example, a meteoroid traveling 60 km/s will form plasma at 120 km if the meteoroid bulk density is small, however a meteoroid traveling at 60 km/s will not form plasma until 95 km if the bulk density is large. This result makes sense in the context of a differential ablation model where the higher density

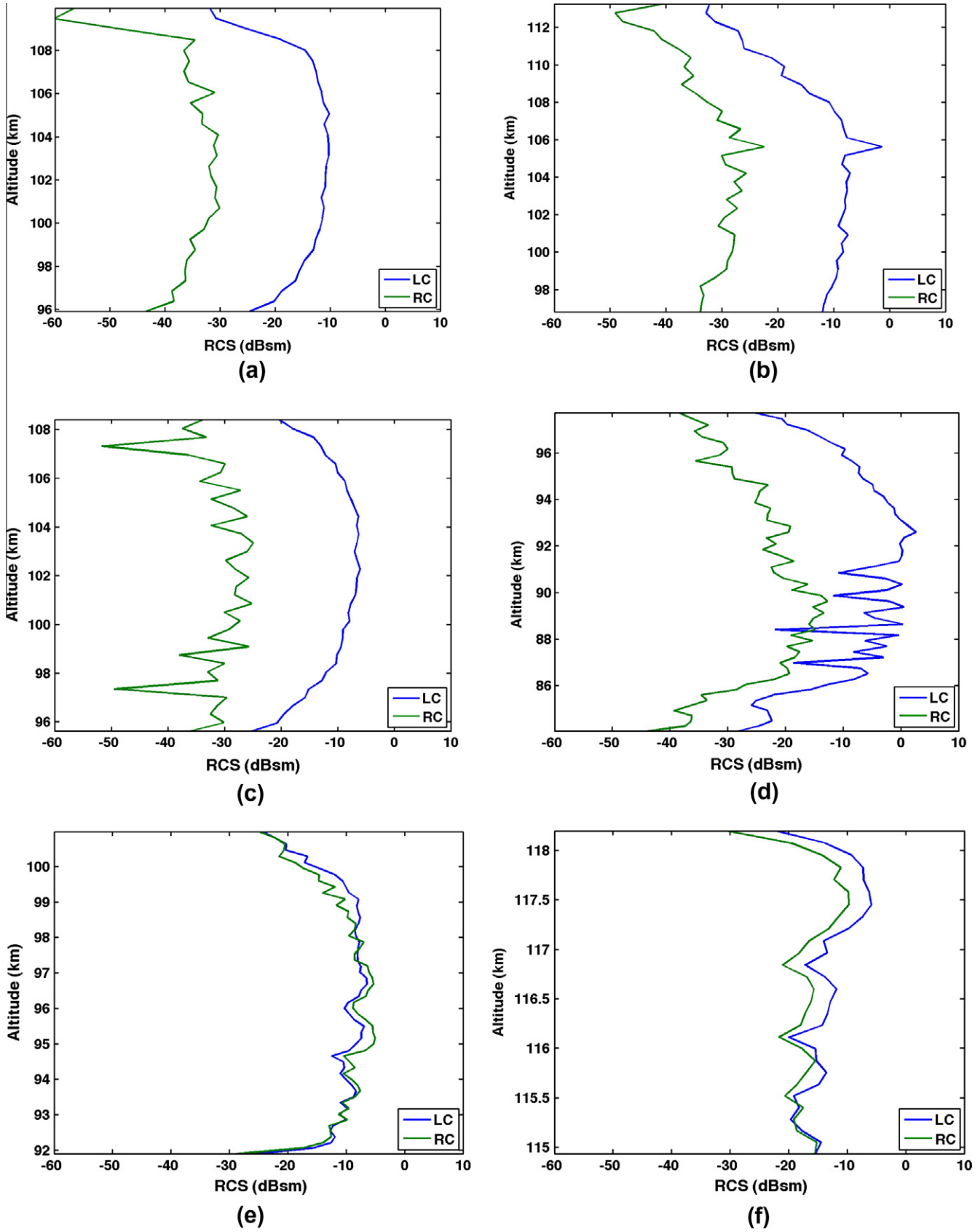

Fig. 3. Representative plots of the left-circular (LC) and right-circular (RC) RCS head echo curves as a function of altitude. These plots show (a) RCS trending with beam pattern with the LC signal stronger than RC, (b) a similar RCS trend with a spike in both polarizations, likely due to differential ablation, (c) a strong and smooth LC curve with the RC signal showing structure, (d) uncorrelated structure in both polarizations with a burst of activity below 90 km in the LC signal only, (e) non-smooth signals in both LC and RC with the signal strengths being approximately equal, and (f) a very slight difference in the signal strengths of LC and RC with what appears to be periodic behavior.

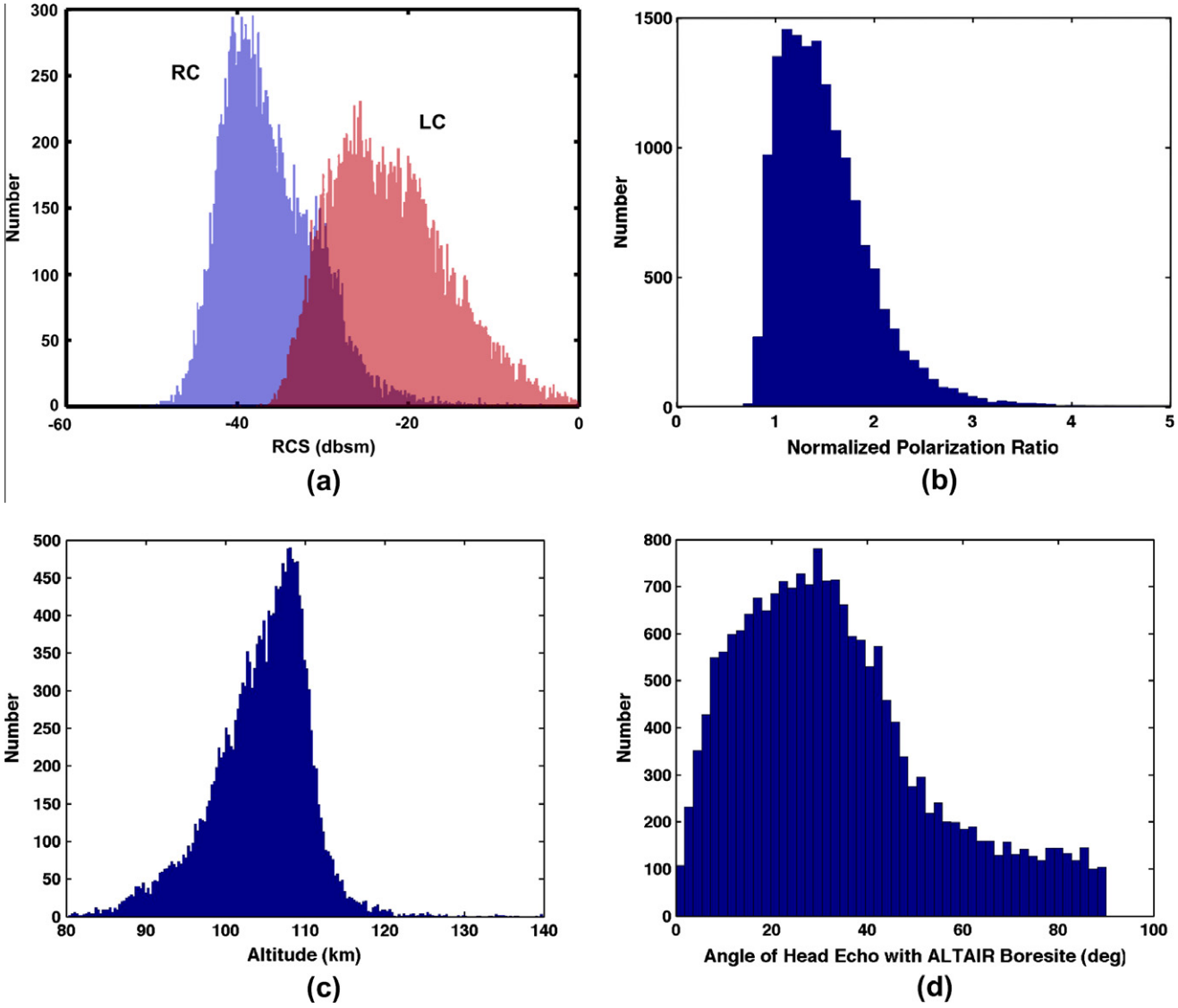

Fig. 4. Histograms for approximately 20,000 VHF head echoes showing number versus (a) RCS for both LC and RC, (b) normalized polarization ratio, (c) altitude, and (d) velocity angle with respect to boresite.

constituents of a meteoroid tend to ablate at higher temperatures and thus at lower altitudes; additionally, it agrees well with Fig. 9 in Janches et al. (2003). We believe the spread in the data in Janches et al. (2003) is actually attributed to the spread in bulk densities, as opposed to errors introduced by assuming that the meteoroids travel parallel to the Arecibo beam. Meteoroids with higher bulk density, containing relatively more high-density constituents, would therefore be expected to ablate and produce significant ionization at lower altitudes.

Without the calculation of both scattering and ballistic masses that we employ to get independent measurements of a meteoroid's mass, radius, and bulk density, there is no known way to measure the density of the meteoroids detected by HPLA radar. Such measurements are vital because HPLA radars can detect meteoroids in a size and speed regime that is unreachable by other techniques. In addition, the dependence that we observe between bulk density and altitude of head echo formation helps constrain theories about how the head echo is formed. This can only help to clear up the ongoing debate about effects such as meteor flares (Mathews et al., 2010) and differential ablation (Janches et al., 2009).

5. Summary and future work

By employing scattering and ionization models (scattering mass) together with conservation of momentum (ballistic mass) and a spherical meteoroid assumption, we have developed an improved technique to independently solve for meteoroid mass, radius, and bulk density from HPLA radar measurements of meteor head echoes. We have applied our technique to dual-frequency (VHF and UHF) data collected in 2007 and 2008 at ALTAIR, which represents approximately 20,000 meteor head echoes. The general approach of independently calculating scattering and ballistic masses is the only known way to measure the bulk density of the small, fast meteoroids detected by HPLA radar, and our density results improve on the previous work of Drew et al. (2004) that first demonstrated this technique. We have observed that high velocity meteoroids tend to create plasma at higher altitudes, while high mass meteoroids result in higher RCS. For a given speed, a meteoroid will generally form plasma at higher altitudes if it is less dense and lower altitudes if it is more dense. Our results are consistent across both frequencies and with other results

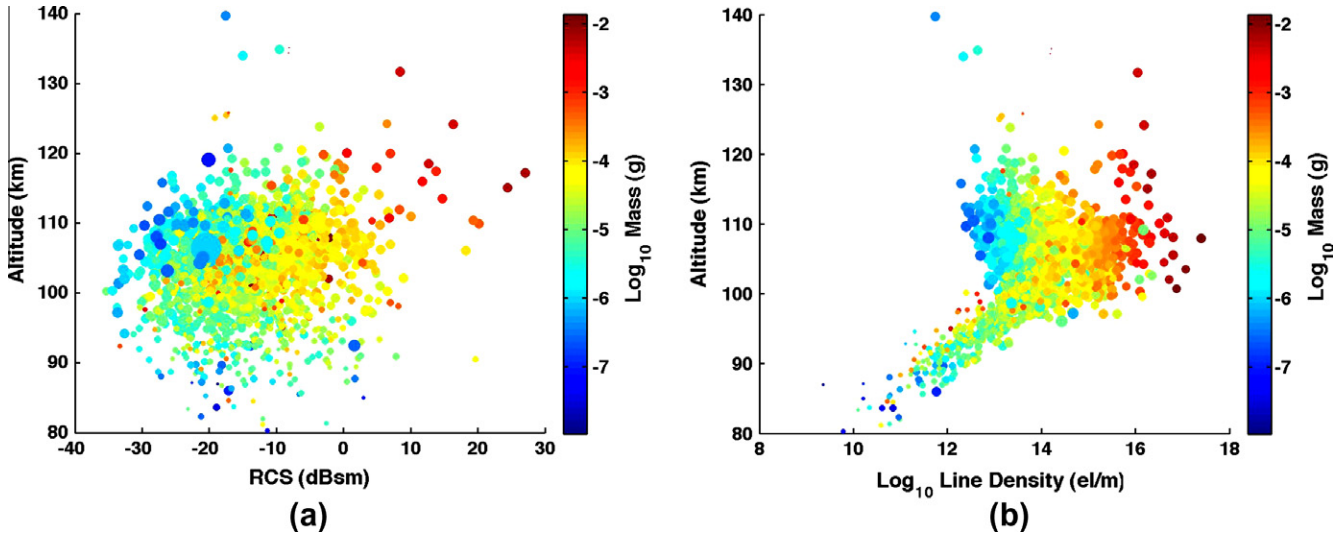

Fig. 5. These data include 2000 VHF head echoes and show (a) LC RCS as a function of altitude, color-coded for scattering mass with circle-size increasing with velocity, and (b) $\log_{10}$ of the line density (in electrons/m) as a function of altitude, color-coded for scattering mass with circle-size increasing with velocity.

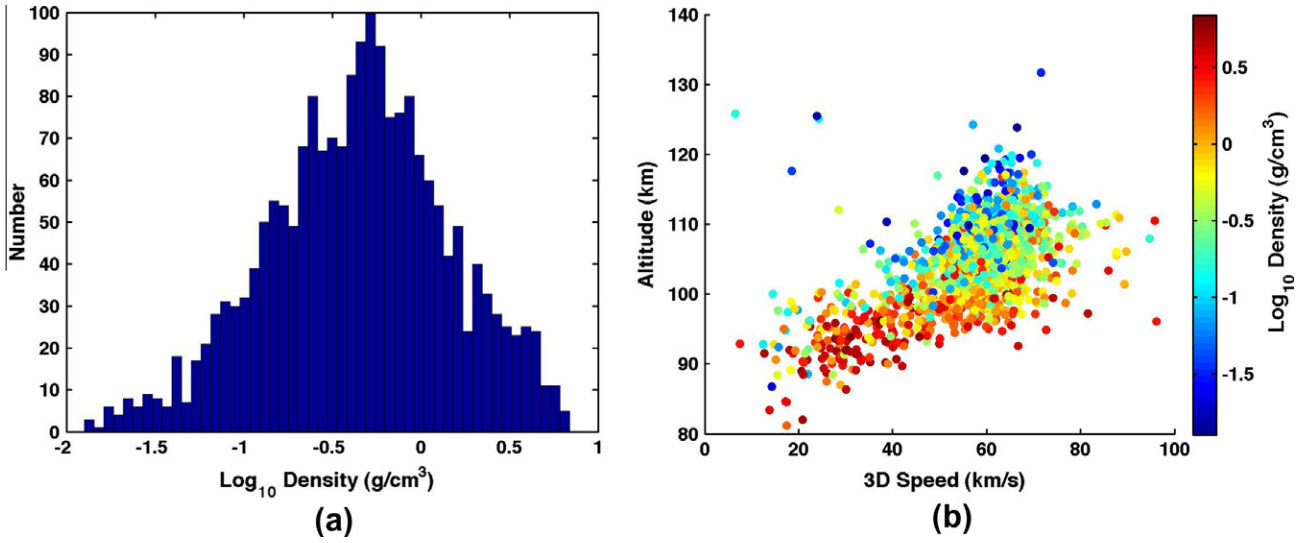

Fig. 6. These data include 2000 VHF head echoes and (a) a histogram of the meteoroid bulk densities and (b) the 3D speed as a function of altitude, color-coded for the $\log_{10}$ of the meteoroid bulk density.

previously reported in the literature, lending confidence in our approach. However, it is also clear that our overall picture of the meteor head plasma formation and scattering processes is far from complete. This was most evident with the comparison between the LC and RC polarization measurements; not only can the polarization ratio vary greatly between head echoes, but most RCS profiles contained sharp variations separate from the beam pattern that were sometimes consistent between polarizations and sometimes not consistent.

Our future work includes improving the scattering model to explain and account for differences between the LC and RC polarizations. Further improvements could come from including a more physically realistic model of the head plasma distribution. Effects such as differential ablation and fragmentation could also be incorporated to explain RCS profile variations. Higher range and range rate resolution through the theory of compressed sensing (Volz and Close, 2011), helpful for studying these effects, will also be an area of future work. All of these would improve the accuracy of our mass, radius, and bulk density estimates. High resolution, dual-polarization, multi-frequency measurements are integral to validation and further development of these models.

Acknowledgments

The authors gratefully acknowledge the contributions from the following people: Dr. William Cooke of the NASA Marshall Space Flight Center sponsored this work.

References

Bass, E., Oppenheim, M., Chau, J., Olmstead, A., 2008. Improving the accuracy of meteoroid mass estimates from head echo deceleration. Earth Moon Planets 102, 379–382.

Chapin, E., Kudeki, E., 1994. Radar interferometric imaging studies of long-duration meteor echoes observed at Jicamarca. J. Geophys. Res. 99, 8937–8949.

Close, S., Hunt, S.M., Minardi, M.J., McKeen, F.M., 2000. Analysis of perseid meteor head echo data collected using the Advanced Research Projects Agency Long-Range Tracking and Instrumentation Radar (ALTAIR). Radio Sci. 35, 1233–1240.

Close, S., Hunt, S., Oppenheim, M., Dyrud, L., 2002. Scattering characteristics of high-resolution meteor head echoes detected at multiple frequencies. J. Geophys. Res. 107.

Close, S., Oppenheim, M., Hunt, S., Coster, A., 2004. A technique for calculating meteor plasma density and meteoroid mass from radar head echo scattering. Icarus 168, 43–52.

Close, S., Oppenheim, M., Durand, D., Dyrud, L., 2005. A new method for determining meteoroid mass from head echo data. J. Geophys. Res. 110.

Close, S., Brown, P., Campbell-Brown, M., Oppenheim, M., Colestock, P., 2007. Meteor head echo radar data: Mass-velocity selection effects. Icarus 186, 547–556.

Close, S., Kelley, M., Vertatschitsch, L., Colestock, P., Oppenheim, M., Yee, J., 2011. Polarization and scattering of a long-duration meteor trail. J. Geophys. Res. 116.

Drew, K., Brown, P.G., Close, S., Durand, D., 2004. Meteoroid bulk density determination using radar head echo observations. Earth Moon Planets 95, 639–645.

Dyrud, L., Janches, D., 2008. Modeling the meteor head echo using Arecibo radar observations. J. Atmos. Solar-Terr. Phys. 70, 1621–1632.

Jackson, J.D., 1975. Classical Electrodynamics. John Wiley & Sons, Inc.

Janches, D.J., Mathews, J.D., Meisel, D.D., Zhou, Q., 2000. Micrometeor observations using the Arecibo 430 MHz radar. Icarus 145, 53–63.

Janches, D., Nolan, M.C., Meisel, D.D., Mathews, J.D., Zhou, Q.H., Moser, D.E., 2003. On the geocentric micrometeor velocity distribution. J. Geophys. Res. 108.

Janches, D., Heinselman, C.J., Chau, J.L., Chandran, A., Woodman, R., 2006. Modeling the global micrometeor input function in the upper atmosphere observed by high power and large aperture radars. J. Geophys. Res. 111.

Janches, D., Close, S., Fentzke, J.T., 2008. A comparison of detection sensitivity between ALTAIR and Arecibo meteor observations: Can high power and large aperture radars detect low velocity meteor head-echoes. Icarus 193, 105–111.

Janches, D., Dyrud, L.P., Broadley, S.L., Plane, J.M.C., 2009. First observation of micrometeoroid differential ablation in the atmosphere. Geophys. Res. Lett., 36.

Jones, W., 1995. Theory of the initial radius of meteor trains. Mon. Not. R. Astron. Soc. 275, 812–818.

Jones, W., 1997. Theoretical and observational determinations of the ionization coefficient of meteors. Mon. Not. R. Astron. Soc. 288, 995–1003.

Kikwaya, J.-B., Campbell-Brown, M., Brown, P.G., 2011. Bulk density of small meteoroids. Astron. Astrophys. 530, http://dx.doi.org/10.1051/0004-6361/201116431.

Love, S.G., Brownlee, D.E., 1993. A direct measurement of the terrestrial mass accretion rate of cosmic dust. Science 262, 550–553.

Loveland, R., Macdonell, A., Close, S., Oppenheim, M., Colestock, P., 2011. Comparison of methods of determining meteoroid range rates from linear frequency modulated chirped pulses. Radio Sci. 46. RS2007.

Mathews, J.D., 2004. Radio science issues surrounding HF/VHF/UHF radar meteor studies. J. Atmos. Solar-Terr. Phys. 66, 285–299.

Mathews, J.D., Meisel, D.D., Hunter, K.P., Getman, V.S., Zhou, Q., 1997. Very high resolution studies of micrometeors using the Arecibo 430 MHz radar. Icarus 126, 157–169.

Mathews, J.D., Briczinski, S.J., Meisel, D.D., Heinselman, C.J., 2008. Radio and meteor science outcomes from comparisons of meteor radar observations at AMISR poker flat, Sondrestrom, and Arecibo. Earth Moon Planets 102, 365–372.

Mathews, J.D., Briczinski, S.J., Malhotra, A., Cross, J., 2010. Extensive meteoroid fragmentation in V/UHF radar meteor observations at Arecibo observatory. Geophys. Res. Lett. 37.

McCausland, P.J.A., Samson, C., McLeod, T., 2011. Determination of bulk density for small meteorite fragments via visible light 3-D laser imaging. Meteorit. Planet. Sci. 46, 1097–1109.

Morse, P.M., Feshbach, H., 1953. Methods of Theoretical Physics, Part II. McGraw-Hill, Inc.

Oppenheim, M.M., Sugar, G., Bass, E., Dimant, Y.S., Chau, J., 2008. Day to night variation in meteor trail measurements: Evidence for a new theory of plasma trail evolution. Geophys. Res. Lett. 35.

Popova, O., 2004. Meteoroid ablation models. Earth Moon Planets 95, 303–319.

Stober, G., Jacobi, C., Singer, W., 2011. Meteoroid mass determination from underdense trails. J. Atmos. Solar-Terr. Phys. 73, 895–900.

Sugar, G., Oppenheim, M.M., Bass, E., Chau, J.L., 2010. Nonspecular meteor trail altitude distributions and durations observed by a 50 MHz high-power radar. J. Geophys. Res. 115.

Szasz, C., Kero, J., Pellinen-Wannberg, A., Meisel, D.D., Wannberg, G., Westman, A., 2008. Estimated visual magnitudes of the EISCAT UHF meteors. Earth Moon Planets 102, 373–378.

Vertatschitsch, L.E., Sahr, J.D., Colestock, P., Close, S., 2011. Meteoroid head echo polarization features studied by numerical electromagnetics modeling. Radio Sci. 46, 9.

Volz, R., Close, S., 2011. A compressed sensing approach to observing distributed radar targets. Paper presented at XXXth URSI General Assembly and Scientific Symposium, Istanbul, Turkey, August 13–20, 2011.

Vondrak, T., Plane, J.M.C., Broadley, S., Janches, D., 2008. A chemical model of meteor ablation. Atmos. Chem. Phys. Discuss. 8, 14557–14606. http://dx.doi.org/10.5194/acpd-8-14557-2008.

Wannberg, G., Pellinen-Wannberg, A., Westman, A., 1996. An ambiguity-function-based method for analysis of Doppler decompressed radar signals applied to EISCAT measurements of oblique UHF–VHF meteor echoes. Radio Sci. 31, 497–518.

Wannberg, G., Westman, A., Pellinen-Wannberg, A., 2011. Meteor head echo polarization at 930 MHz studied with the EISCAT UHF HPLA radar. Ann. Geophys. 29, 1197–1208.

Westman, A., Wannberg, G., Pellinen-Wannberg, A., 1997. Meteor head echo height ceiling effect observed by the European incoherent scatter UHF and VHF radars. J. Geophys. Res.

Westman, A., Wannberg, G., Pellinen-Wannberg, A., 2004. Meteor head echo altitude distributions and the height cutoff effect studied with the EISCAT HPLA UHF and VHF radars. Ann. Geophys. 22, 1575–1584.

Zhou, Q.H., Perillat, P., Cho, J.Y.N., Mathews, J.D., 1998. Simultaneous meteor echo observations by large aperture VHF and UHF radars. Radio Sci. 33, 1641–1654.